Biomicrofluidics ARTICLE pubs.aip.org/aip/bmf

Impact of dcEF on microRNA profiles in glioblastoma and exosomes using a novel microfluidic bioreactor

Cite as: Biomicrofluidics 18, 064106 (2024); doi: 10.1063/5.0228901
Submitted: 16 July 2024 · Accepted: 26 November 2024 ·
Published Online: 27 December 2024

Hsieh-Fu Tsai[1,a)] and Amy Q. Shen[2,a)]

AFFILIATIONS

[1]Department of Biomedical Engineering, Chang Gung University, Taoyuan City 333, Taiwan and Department of Neurosurgery, Chang Gung Memorial Hospital, Keelung, Keelung City 204, Taiwan
[2]Micro/Bio/Nanofluidics Unit, Okinawa Institute of Science and Technology Graduate University, Onna-son, Okinawa 904-0495, Japan

Note: This paper is part of the special collection, Selected Papers from IEEE-NANOMED 2023.
a)Authors to whom correspondence should be addressed: hftsai@cgu.edu.tw and amy.shen@oist.jp

ABSTRACT

Glioblastoma multiforme, the most common type of highly aggressive primary brain tumor, is influenced by complex molecular signaling pathways, where microRNAs (miRNAs) play a critical regulatory role. Originating from glial cells, glioblastoma cells are affected by the physiological direct current electric field (dcEF) in the central nervous system. While dcEF has been shown to affect glioblastoma migration (electrotaxis), the specific impact on glioblastoma intercellular communication and miRNA expression in glioblastoma cells and their exosomes remains unclear. This study aims to fill this gap by investigating the differential expression of microRNAs in glioblastoma cells and exosomes under dcEF stimulation. We have developed a novel, reversibly sealed dcEF stimulation bioreactor that ensures uniform dcEF stimulation across a large cell culture area, specifically targeting glioblastoma cells and primary human astrocytes. Using microarray analysis, we examined differential miRNA profiles in both cellular and exosomal RNAs. Our study identified shared molecular targets and pathways affected by dcEF stimulation. Our findings reveal significant changes in miRNA expression due to dcEF stimulation, with specific miRNAs, such as hsa-miR-4440 being up-regulated and hsa-miR-3201 and hsa-mir-548g being down-regulated. Future research will focus on elucidating the molecular mechanisms of these miRNAs and their potential as diagnostic biomarkers. The developed platform offers high-quality dcEF stimulation and rapid sample recovery, with potential applications in tissue engineering and multi-omics molecular analysis.

I. INTRODUCTION

In multicellular organisms, tissue polarity creates trans-epithelial potential differences that drive a physiological direct current electric field (dcEF).[1–3] These fields play critical roles in early embryonic development[4,5] and wound healing.[6–9] Physiological electric fields act as directional cues for cell recruitment and migration, known as electrotaxis or galvanotaxis,[10,11] and may also contribute to cancer metastasis.[12–14] Despite their importance, the molecular mechanisms underlying dcEF-induced cell recruitment remain poorly understood, largely due to the complexity of signaling cascades triggered by localized ionic currents.[15]

Glioblastoma multiforme (GBM) is an aggressive brain tumor originating from astrocytes, a type of glial cells in the central nervous system (CNS), which are influenced by local field potentials from neuronal action potentials.[16,17] GBM cells can aggressively diffuse in a nearby tissue and metastasize into secondary tumors but rarely disseminate outside the CNS.[18,19] Intermediate frequency alternating current electric fields have shown antimitotic efficacy on glioblastoma cells and are used in the Food and Drug Administration (FDA)-approved tumor-treating-field therapy.[20]

Beyond physical voltage gradients, cells communicate through remote chemical signaling via exosomes—40–150 nm

microvesicles secreted into the microenvironment that mediate intercellular communication.[21,22] Exosomes carry potent cargo, such as lipids, proteins, and nucleic acids, including microRNAs (miRNAs).[23] MiRNAs are small non-coding RNAs that play a pivotal role in the gene expression regulatory network, also known as the regulome, by targeting messenger RNAs in cells.[24] Exosomal miRNAs play significant roles in cancer pathogenesis and tumor microenvironment signaling, making them important biomarkers.[25–28]

Conventionally, conductive electrodes in configurations, such as wires and plates, are employed for electrical stimulation in tissue engineering on commercial platforms.[29–32] While these electrodes are easy to implement, they often generate highly non-uniform electric fields, with a coefficient of variation (CV) as high as 51.6%.[33] Such non-uniform fields can lead to inconsistent tissue stimulation and increased cell death.

Microfluidic technology has become an extremely effective tool in biomedical research, particularly for isolating and detecting exosomes and exosomal miRNAs. However, conventional microfluidic devices typically yield insufficient sample quantities for multi-omics studies.[34] Microfluidic bioreactors, on the other hand, offer large culture areas and provide advantages, such as increased sample yield, precise electrical stimulation, controlled perfusion, reduced reagent use, and compatibility with microscopy.[35–37] State-of-the-art microfluidic bioreactors feature large rectangular microchannels with small cross sections, enabling uniform dcEFs across 18–69 cm^2 culture areas with a CV as low as 1.2%, while minimizing Joule heating.[38,39]

However, state-of-the-art microfluidic bioreactors still often rely on irreversible sealing methods, such as adhesive tapes or plasma treatment, to prevent leakage when integrating with a cell culture apparatus. The irreversible sealing complicates sample recovery and can limit experimental flexibility.[38] While Tsai *et al.* developed a snap-off device where the microfluidic chamber could be pried open to access the cellular products,[39] this method could introduce mechanical shears to the cells and cause sample loss. Furthermore, cells delivered into assembled chips may also settle in unintended locations, such as dead spaces or tubing, potentially influencing biological outcomes when collecting samples.

This study investigates miRNA expression in glioblastoma cells and exosomes under dcEF stimulation. While the transcriptome of dcEF-stimulated cells has been explored,[38,40,41] existing studies on miRNA differential expression under electrical stimulation are limited to pulsed dcEF,[42–47] alternating current electric fields,[48] and extremely low-frequency electromagnetic fields.[49] To address the need for uniform dcEF stimulation and RNA integrity, we developed a robust large-area dcEF stimulation bioreactor that reduces handling time compared to previous designs.[39] This bioreactor, cultured in a physioxia-mimicking environment, enables easy collection of total RNA from cells and exosomes. We then analyzed the differential expression of miRNAs using microarray technology to identify specific miRNAs affected by dcEF stimulation. Our findings provide new insights into the molecular targets and pathways influenced by dcEF, with potential implications for diagnostic biomarker development and therapeutic strategies.

II. MATERIALS AND METHODS

A. Cell culture and maintenance

Glioblastoma cell lines U251MG (IFO50288, Japanese Cancer Resources Bank, Japan) and T98G (CRL-1690, American Type Culture Collection, ATCC, USA) were obtained from respective biobanks and thawed according to the provided instructions. Ethical approval was not required. U251MG and T98G cells were cultured in minimum essential media alpha (MEMα) supplemented with 10% fetal bovine serum (FBS) under a 37 °C, 5% CO_2, 5% O_2 moist physioxia atmosphere (i160, Forma Steri-Cycle, Thermo Fisher Scientific, USA). Cryopreserved human astrocytes (N7805, Gibco, Thermo Fisher Scientific, USA) were cultured in astrocyte medium composed of DMEM and 10% FBS and 1% N-2 supplement (Thermo Fisher Scientific, USA) under the same environment. All cells were subcultured every other day or whenever the cell confluency reached 80% using TrypLE recombinant trypsin (Thermo Fisher Scientific, USA). The cells were checked against mycoplasma contamination using species-specific polymerase chain reactions (PCRs) (EZ-PCR kit, Sartorius, Germany) on a thermocycler (T100, Bio-Rad, USA). All cells used in the experiment were within the fifth to ninth generations. Frozen cell stocks, except for primary astrocytes, were prepared by resuspending 1×10^6 log-phase cells in a 1 ml CellBanker solution (Takara Bio, Japan) and cooled down in a freezing container (Nalgene, USA) in −80 °C overnight. The frozen cells were then stored in the aqueous phase of liquid nitrogen.

B. Microfluidic bioreactor design and fabrication

The microfluidic bioreactor consisted of a top assembly made from polymethyl methacrylate (PMMA), a fluoro-rubber o-ring, a borofloat glass, and a 0.1 mm-thick tape sealing the 74×40 mm^2 (L × W) culture area. The top PMMA assembly comprised two top PMMA pieces, holding inlets, outlets, and salt bridge connections, two middle plates containing current rectifying chambers (CRCs), and a bottom plate [Fig. 1(a)]. The salt bridge (SB) connection openings were positioned around 10 mm from the edges of the current rectifying chambers. The dcEF distribution in the bottom cell culture chamber was numerically simulated using finite element methods (electric current module, COMSOL Multiphysics, USA). The electrical current to build 100 V m^{-1} dcEF in the cell microchannel was set as the boundary condition on the salt bridges for the simulation.

The components for the top PMMA assembly were fabricated using a CO_2 laser cutter (VLS3.50, Universal Laser Systems, USA) to cut patterns designed in AutoCAD (Autodesk, USA) from a 3 mm-thick PMMA sheet (cast acrylic sheet K, Kanase, Japan). The bottom plate featured a 2 mm-wide, 1.8 mm-deep slot with a perimeter of ≈268 mm, milled using a computer numerical control micro mill (SLS Micro Mill/GX, Minitech, USA). For computer-aided machining, tool paths were generated using Fusion software (Autodesk, USA). The top pieces and current rectifying chamber plates were thermally bonded and affixed to the bottom plate using a cyanoacrylate adhesive (406, Loctite, Germany). M6-threaded polycarbonate adapters were attached to the top pieces using a cyanoacrylate adhesive (NBK, Japan). A 2 mm-thick fluoro-rubber

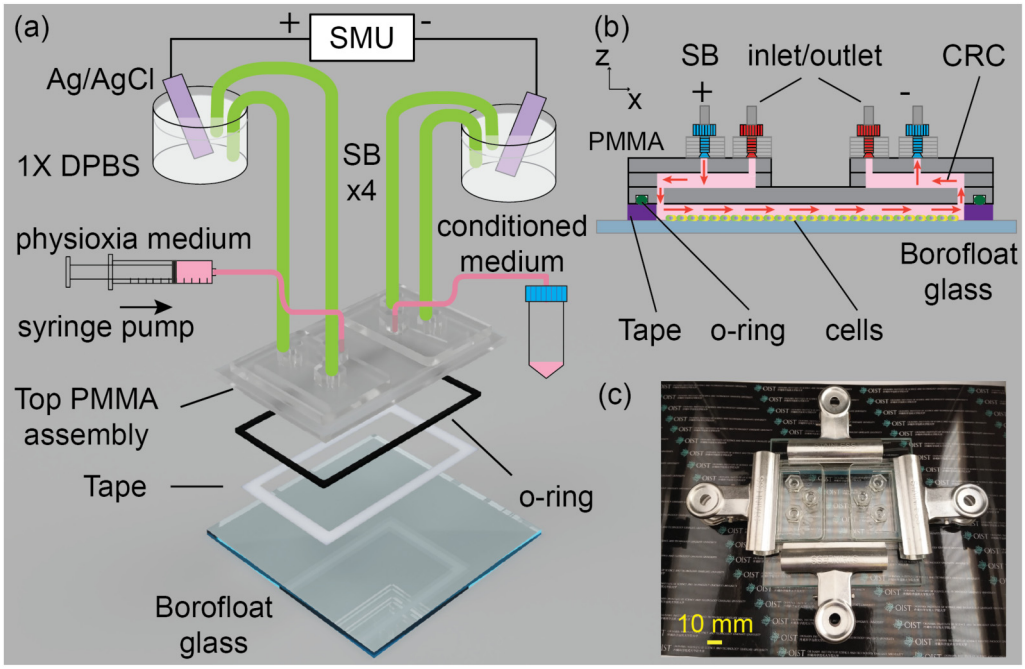

FIG. 1. The reversibly sealed dcEF bioreactor. (a) Diagram of the experimental setup. DPBS, Dulbecco's phosphate buffered solution; SB, salt bridges; and SMU, source-measure-unit. (b) Cross section in the *x*–*z* plane depicts the bioreactor channel layout. The electrical current flow is shown in red arrows. CRC, current rectifying chamber. (c) Snapshot showing the assembled bioreactor without tubing. The scale bar represents 10 mm in length.

o-ring with an inner diameter of 84.5 mm (4DS85, NOK, Japan) was placed in the micro-milled slot to complete the top PMMA assembly fabrication process. Before experiment use, the top PMMA assembly underwent ultraviolet (UV) disinfection for a minimum of 12 h.

C. Implementation of dcEF stimulation

Assembly and disassembly operations were conducted in an ISO class 1 cleanroom environment established by laminar flow units (KOACH T500, KOKEN Ltd., Japan), maintaining a spacing of 65 cm at an airflow rate of 0.4 m s^{-1}. The cleanliness of the environment was verified using a particle counter (MET ONE HHPC3+, Beckman Coulter, USA).

Initially, a 2 mm-thick borofloat glass (Schott, Germany), encased with a CO_2 laser-cut 8018PT tape (liner-unremoved, 0.1 mm-thick, 3M, USA) around the microfluidic chamber, underwent UV disinfection for 2 h. Subsequently, the glass bottom was coated with a 2 ml Geltrex solution (0.13 mg mL^{-1}, A1569601, Thermo Fisher Scientific, USA) and incubated for 2 h in a cell culture incubator. Following this, 5×10^5 cells were uniformly seeded within the chamber enclosed by the 8018PT tape and incubated for 3 h under physioxia conditions (5% CO_2 and 5% O_2). Syringes (Terumo, Japan) were then connected to the top PMMA assembly through fittings and tubings (IDEX Health & Science, USA). Salt bridge tubes that were comprised of 1/8″-inner-diameter Tygon tubes with 1% agarose in Dulbecco's phosphate buffered saline (DPBS) were connected to the top PMMA microdevice (LE agarose, Lonza, USA). The CRCs were filled with experimental media (cell culture medium with 5% exosome-depleted FBS). The experimental media were also pre-equilibrated in the physioxia environment in an air-permeable flask for at least 8 h.

Next, the top PMMA assembly was sealed against the 0.1 mm-thick 8018PT tape on the borofloat glass containing cells through a submersion process to avoid bubble formation on a clean bench. Specifically, the borofloat glass with cells in the chamber was submerged in a sterilized polypropylene container with sufficient DPBS to submerge the top PMMA assembly. The aforementioned top PMMA assembly was then submerged and sealed with the borofloat glass after no visible bubble was trapped in the chamber. Four clamps securely clamped the top PMMA microdevice with the borofloat glass by deforming the o-ring against the 8018PT tape, thereby sealing the cell chamber into a microchannel and completing the bioreactor [Figs. 1(b) and 1(c)].

Finally, the assembled bioreactor was removed from the DPBS solution, and the DPBS in the bioreactor was replaced with the experimental medium by perfusing with a syringe pump (YMC, Japan) for 10 min at 250 μl min^{-1}. Afterward, 100 V m^{-1} dcEF stimulation was applied to cells for 48 h by sourcing a fixed current through two 15×10 cm^2 (L×W) silver/silver chloride (Ag/AgCl) electrodes in 1× DPBS through a precision source/measure unit (SMU, B2902A, Keysight, USA) (Fig. 1). The experimental medium was steadily perfused at 250 μl h^{-1} for the duration, and the conditioned medium was collected at the outlet. The sham (control)

samples were conducted simultaneously with their dcEF-stimulated counterparts (all treatments were the same except no current was sourced).

The electrical conductivities of the MEMα medium with 5% FBS and an astrocyte medium with 5% FBS were measured using a conductivity probe (3552-10D, Horiba, Japan) and found to be 1.515 ± 0.021 and 1.602 ± 0.032 (mean $\pm$ standard deviation, S m^{-1}) at 37 °C. Accordingly, the electrical current applied by the SMU for 100 V m^{-1} dcEF stimulation on glioblastoma cells or astrocytes in the $74 \times 40 \times 0.1$ mm^3 (L×W×H) microchannel can be calculated using Eq. (1) as approximately 606 and 640 μA, respectively,

$$I = \mathrm{EFS} \times \sigma \times \mathrm{W} \times \mathrm{H}, \tag{1}$$

where σ is the electrical conductivity (S m^{-1}), W is the microchannel width (mm), and H is the microchannel height (mm).[50]

All experiments were performed in duplicates with an applied voltage of approximately 28 V. A photograph of the dcEF stimulation setup is provided in Fig. S1 of the supplementary material.

D. Isolation and purification of exosomes and RNA

After applying the dcEF stimulation or sham treatment without dcEF, the dishes containing the devices were placed on ice. The PMMA microdevice was then disassembled by removing the clamps, and the conditioned medium from the device was collected along with the medium collected at the outlet. The workflow is shown in Fig. 2(a).

The cells at the glass bottom were immediately washed with ice-cold 1× DPBS and then collected by scrapers (Nunc, Thermo Fisher Scientific, USA). The exosomes were purified through a series of differential centrifugation steps at 300×g for 10 min, 1000×g for 10 min, and 10 000×g for 45 min at 4 °C in a centrifuge (MX-301, TOMY, Japan). After each step, the supernatant solution was transferred to a new tube. Subsequently, the exosomes were concentrated at 235 000×g for 2 h on an ultracentrifuge equipped with an SW-40Ti rotor (Optima L-100XP, Beckman Coulter, USA). The exosomes were promptly fixed for electron microscopy observation or advanced to total RNA extraction.

For the total RNA extraction, the mirVana RNA isolation kit (Thermo Fisher Scientific, USA) was employed following the manufacturer's guidelines within the ISO class one clean space. The DPBS-washed cells or an exosome pellet were lysed in a 600 μl lysis/binding buffer and mixed with a 60 μl homogenate additive and 660 μl acid-phenol chloroform. Following proper mixing and 10 000 ×g centrifugation, the total RNAs in the aqueous phase were isolated and further processed by adding 0.1 mg glycogen and 1.25 (v/v) 100% ethanol and binding through glass fiber filters. Finally, the total RNAs underwent washing and elution in nuclease-free water.

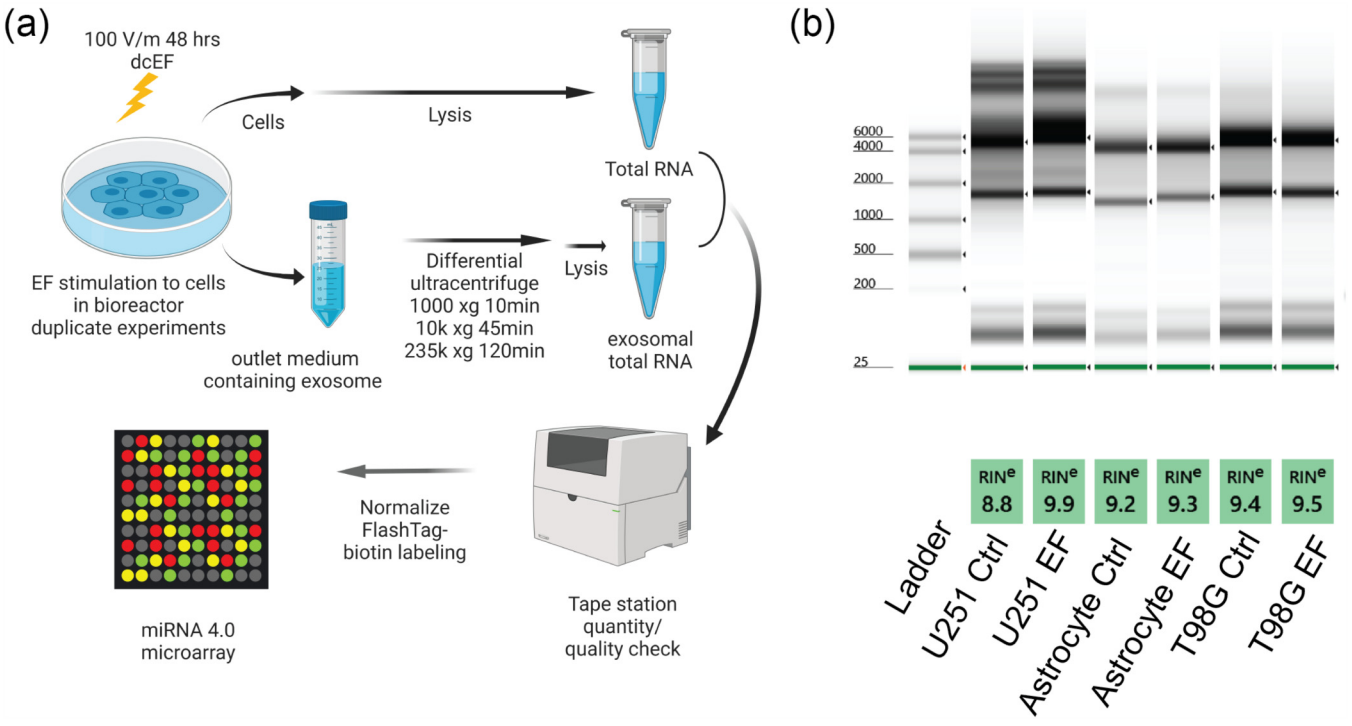

FIG. 2. Overview and RNA quality assessment of the microarray experiment. (a) Schematic workflow of the miRNA microarray experiment, created with BioRender.com. (b) Quality evaluation of total cellular RNA using the Agilent TapeStation 4200.

The total RNA quality was evaluated using nanodrop spectrophotometry (Nanodrop2000, Thermo Fisher Scientific, USA) and a high-sensitivity RNA capillary gel electrophoresis assay (TapeStation 4200, Agilent, USA) and stored in −80 °C until biotin tagging. Total RNAs from cell samples were confirmed to have an RNA integrity number (RIN) above seven, while the total RNAs from exosomal samples were unreliable due to a lack of large RNAs [see Fig. 2(b)]. The total cell RNA quantifications from TapeStation were used for sample amount normalization in downstream biotin tagging and microarray hybridization, whereas total RNA from exosomes was quantified using a nanodrop spectrophotometer.

E. Electron microscopy

The purified exosomes were fixed with 100 μl of 2% paraformaldehyde and loaded on carbon film-coated 200 mesh copper electron microscopy (EM) grids (Nisshin EM Co., Ltd., Japan). The grids were counter-stained with 1% uranyl acetate (Sigma-Aldrich, USA), washed, and dried. The exosomes on the EM grids were imaged at 100 keV on a transmission electron microscope (JEOL1400 Flash, JEOL Ltd., Japan).

F. Comprehensive microRNA microarray profiling

In accordance with the manufacturer's protocol, duplicate total RNA samples were pooled before biotin labeling using the FlashTag HSR RNA labeling kit (Thermo Fisher Scientific, USA). Approximately 130 ng of biotin-tagged samples, along with hybridization controls, were loaded into GeneChip miRNA 4.0 microarray cartridges (array format type 100, Thermo Fisher Scientific, USA) and hybridized for 18 ± 0.5 h at 48 °C with 60 rpm rotation in GeneChip Hybridization Oven 645. Cartridges were subsequently washed using the GeneChip Fluidics Station 450 as per the manufacturer's instructions.

Following hybridization and washing, the cartridges were scanned using a GeneChip scanner (3000 7G, Thermo Fisher Scientific, USA), and the resulting data were analyzed using Transcriptome Analysis Console (TAC) software (Thermo Fisher Scientific, USA).

G. Microarray data analysis

The CEL files were imported, and miRNA QC tools were used to assess the quality of the array data using all the hybridization and spike-in controls. The data were normalized by the robust microarray analysis (RMA) and detection above background (DABG) methods with human-only probe sets in the TAC software algorithms.

A comparative analysis between dcEF-stimulated samples and control (sham) samples was carried out using a log2 fold change (FC) > 1. A probeset was considered expressed if more than 50% samples had DABG values below the threshold of 0.05. Differential expression was statistically calculated using an eBayes algorithm. A P value smaller than 0.05 indicates that a probe set has fold changes rejecting the null hypothesis at a 95% confidence level.[51] Hierarchical clustering was conducted using complete linkage and Euclidean distance as the similarity measure for the differentially expressed miRNAs. Comparisons of cell and exosomal samples of all three cell types between dcEF vs sham (Ctrl) were conducted as the overall comparison. Separate analysis comparing in cell samples between EF vs sham and exosomal samples between EF vs sham was also performed in the separate comparison.

Pathways associated with identified miRNAs were analyzed unidirectionally against pathway databases using the miRTargetLink 2.0 platform,[52] considering both weakly and strongly validated targets.

III. RESULTS

A. Uniform dcEF stimulation enabled by 3D microfluidic design

Careful 3D design of the current rectifying chamber [see CRC in Fig. 1(b)] ensures the creation of a uniform dcEF for cell stimulation in the reversibly sealed bioreactor.

The electric current is evenly distributed within the rectifying chamber before entering the cell culture chamber through a slit in the bottom plate [Fig. 1(b)], ensuring a uniform electric field. This uniformity is crucial to minimize dielectrophoresis effects and provide consistent electrical stimulation to the cells.

To establish a DC electric field (dcEF) of 100 V m^{-1}, we simulated a DC electrical current input from salt bridges. The electric field strength (EFS) measured at 5 μm was 98.89 ± 0.07 V m^{-1} (mean ± standard error of mean); see Fig. S2 in the supplementary material. The CV of dcEF calculated within the area with a 500 μm margin to the boundary of the chip was 5.2%. It was slightly larger due to the higher chamber height but comparable to the 1.2%–1.3% reported by Tsai *et al.* and in an other large culture area dcEF stimulation device.[33,38,39,37] In comparison, the CV of the dcEF created by simple wires in a conventional system[30] was simulated to be 51.6%, and the CV of the dcEF created by plate electrodes in a conventional electrical pacing system[53] was simulated to be 39.4%.

B. Enhanced sample recovery with a reversibly sealed dcEF bioreactor

Microfluidic technology has become an extremely effective tool to study cell behaviors in a controlled microenvironment, particularly in bioelectricity contexts.[35,36] The small cross section of a microfluidic channel allows for the creation of physiological-strength dcEF using standard laboratory power supplies, with minimal Joule heating. Moreover, rectangular microchannels facilitate the creation of uniform dcEFs.

However, traditional microfluidic devices often require irreversible sealing methods, such as adhesive tapes or plasma treatment, to prevent leakage when integrating with a glass bottom. Despite their advantages in low reagent consumption, minimal cell quantities, and compatibility with microscopy setups, dcEF stimulation devices suffer from limited sample recovery for downstream molecular analysis and challenges in accessing samples cultured within the device.[38,39] Cells delivered into assembled chips may also settle in unintended locations, such as dead spaces or tubing, potentially influencing biological outcomes when collecting samples.

In our proposed reversibly sealed dcEF bioreactor, cells are seeded and allowed to adhere to the bottom of the culture chamber. The top PMMA assembly seals the microchannel reversibly through simple clamping in a buffer solution, effectively preventing bubble formation that can cause cell death and loss due to shear forces within microchannels (see Fig. 3). Our experiments demonstrate no leakage under perfusion rates up to 1 ml min^{-1}.

Following dcEF stimulation experiments, the top PMMA assembly can be easily removed by unclamping [see Fig. 1(c)]. The cells and the conditioned medium within the channel can be collected promptly with a minimal dwell time. In our experiments, 1.8–3.8 μg of total cellular RNA can be collected from one experiment, varied by cell types. Exosomes can be isolated in the conditioned medium collected from the outlets by differential centrifugation [see Fig. 2(a)]. The quality of cellular total RNA is assessed using capillary gel electrophoresis on TapeStation, consistently showing high quality suitable for microarray analysis (above seven) [see Fig. 2(b)]. The exosomes released from the cells can be identified from transmission electron microscopy imaging (see Fig. 4).

C. Identification of small RNAs regulated by dcEF stimulation in cellular and exosomal RNAs

The principal component analysis of the samples is shown in Fig. S3 of the supplementary material. While miRNA expression profiles are similar between sham and dcEF-stimulated samples, exosomal samples exhibit distinct profiles compared to total cellular samples.

Normalized comparative analysis of miRNA expression between dcEF stimulation and sham reveals 881 small RNAs identified in cellular RNA and 1529 in exosomal RNA (see Fig. 5). The miRNAs expressed in both cellular and exosomal samples were further analyzed by a group comparison between dcEF and sham. Scatterplots and volcano plots of miRNAs with P values less than 0.05 and fold changes greater than 2 or less than −2 are presented in Fig. S4 of the supplementary material.

A total of 16 small RNAs (excluding a duplicated target) are identified, rejecting the null hypothesis due to dcEF stimulation (Table I). The hierarchical clustering of these small RNAs is shown in Fig. 6(a).

We also performed separate analyses between cellular RNA samples and the exosomal RNA samples. The small RNAs in double or triple intersect (93) in cellular total RNAs between dcEF compared to their sham in all three cell types were analyzed. Those small RNAs (374) from exosomal RNAs were also identified (see Fig. 5).

Twenty-one miRNAs were found to express in both cellular RNA and exosomal RNA samples (Table S1 in the supplementary material). The hierarchy clustering of the 21 miRNAs is shown in Fig. 6(b).

Among the dcEF to sham overall comparison analysis and separate analysis between cellular RNA and exosomal RNA, two miRNAs and one stem-loop RNA were found in both analyses (hsa-miR-3201, hsa-miR-4440, hsa-mir-548 g). hsa-miR-4440 is up-regulated (−3.03-fold, $P = 0.0009$), whereas hsa-miR-3201 (5.39-fold, $P = 0.0253$) and hsa-mir-548 g (2.01-fold, $P = 0.0288$) are down-regulated (Table I).

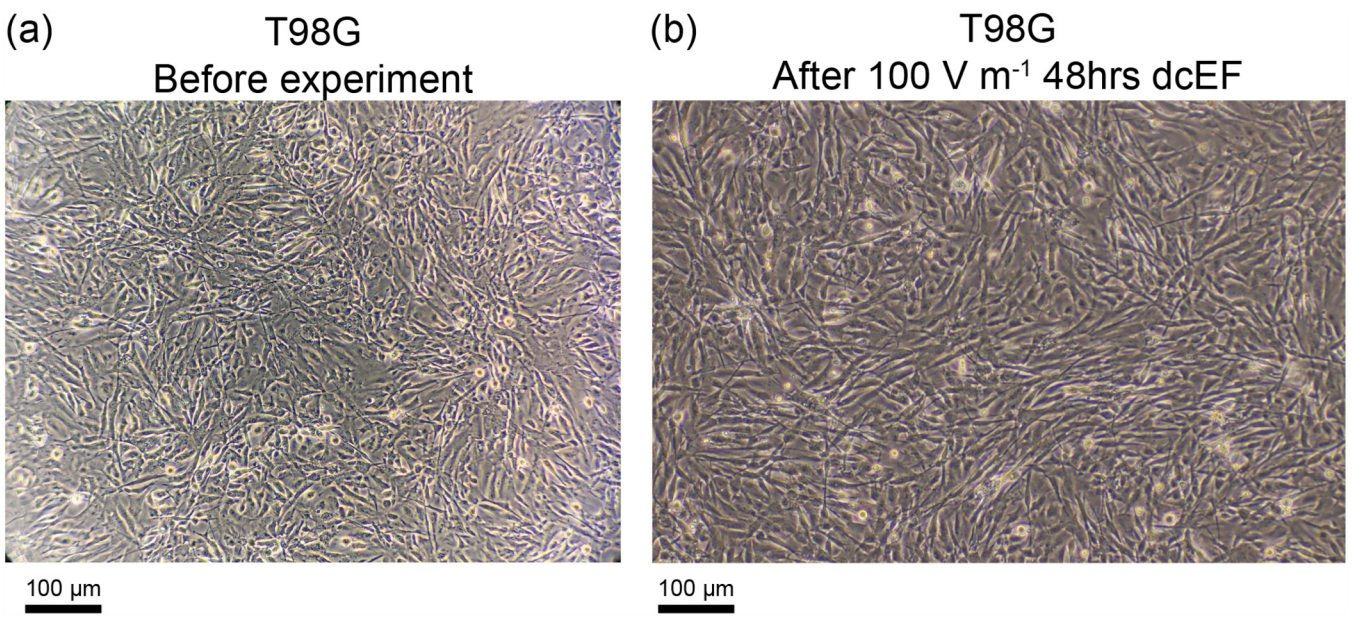

FIG. 3. The phase contrast microscopy images of T98G cells (a) before and (b) after 100 V m^{-1} 48 h dcEF stimulation. No visible change in cell morphology was observed.

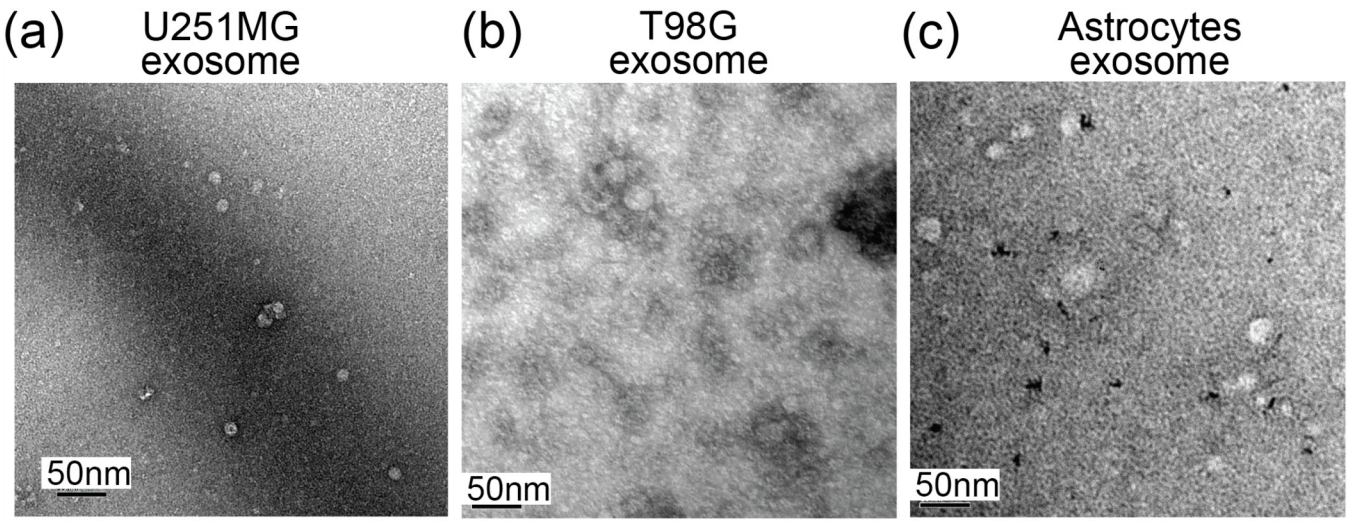

FIG. 4. Transmission electron micrographs showing purified exosomes derived from (a) U251MG glioblastoma cells, (b) T98G glioblastoma cells, and (c) astrocytes. The scale bars represent 50 nm.

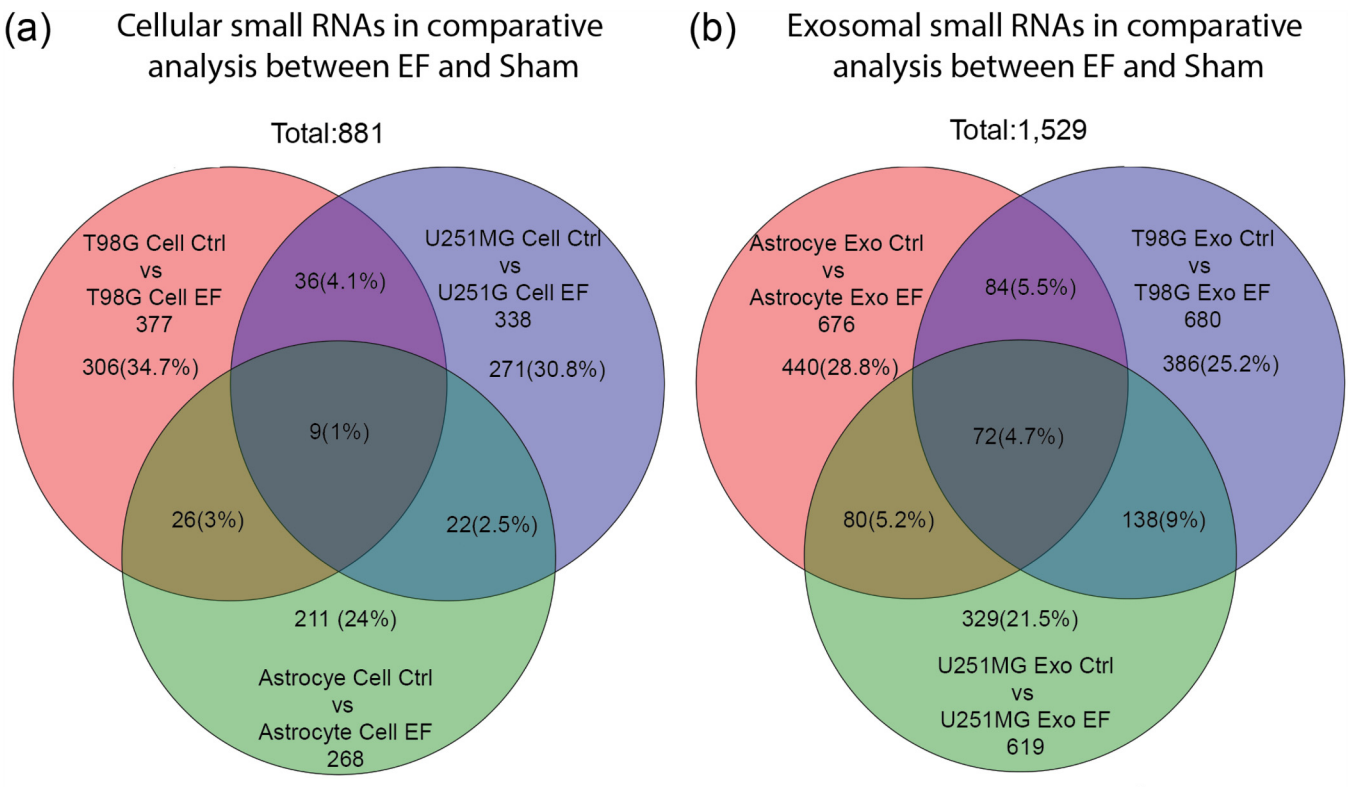

FIG. 5. The Venn diagrams of miRNA microarray results from (a) cellular RNA and (b) exosomal RNA in three cell types after 100 V m^{-1} dcEF stimulation.

TABLE I. The relative expression of small RNAs in analysis of ensemble cellular and exosomal RNA compared between dcEF and sham (Ctrl) samples. Boldface denotes the small RNAs that are identified in both overall comparison and separate comparison analysis.

Transcript ID	ID	sham Avg (log2)	dcEF Avg (log2)	Fold change	P-val	Sequence type
hsa-miR-4440	20518815	1.49	3.09	3.03	0.0009	miRNA
ENSG00000253014	20534093	2.72	1.56	−2.25	0.0102	snoRNA
ENSG00000201009	20532829	2.51	1.33	−2.28	0.012	snoRNA
U46	20538187	2.51	1.33	−2.28	0.012	C/DBox
hsa-miR-1272	20506868	4.92	3.18	−3.35	0.0163	miRNA
ENSG00000239126	20533735	5.73	4.45	−2.43	0.0178	snoRNA
ENSG00000252277	20533921	6.38	4.03	−5.12	0.0187	snoRNA
14qII-29	20532603	2.06	0.56	−2.84	0.024	C/DBox
hsa-miR-3201	20515646	3.86	1.43	−5.39	0.0253	miRNA
hsa-miR-6875-5p	20525711	1.38	2.7	2.49	0.0256	miRNA
hsa-mir-548g	20535875	3.02	2.02	−2.01	0.0288	stem-loop
hsa-miR-542-3p	20504435	2.69	1.41	−2.42	0.0315	miRNA
HBII-85-26	20534320	8.81	6.3	−5.68	0.0379	C/DBox
hsa-miR-7111-5p	20526180	0.99	2.41	2.67	0.0387	miRNA
hsa-mir-3910-1	20536607	4.12	3.02	−2.16	0.041	stem-loop
ENSG00000252277	20533922	6.09	4.05	−4.12	0.0067	snoRNA

We further performed the pathway analysis with the 21 miRNAs identified separately by analyzing cellular RNAs or exosomal RNAs [Fig. 7(b) and Table S1 in the supplementary material). Fourteen gene targets were identified by finding targets with connections to a minimum of five miRNAs, including *ZNF460*, *KLHL15*, *MIDN*, *ARL5B*, *ZNF678*, *ANP32E*, *FAM49A*, *NWD1*, *MIER3*, *FEM1A*, *RREB1*, *BRMS1L*, *ARIH1*, and *PITPNC1*.

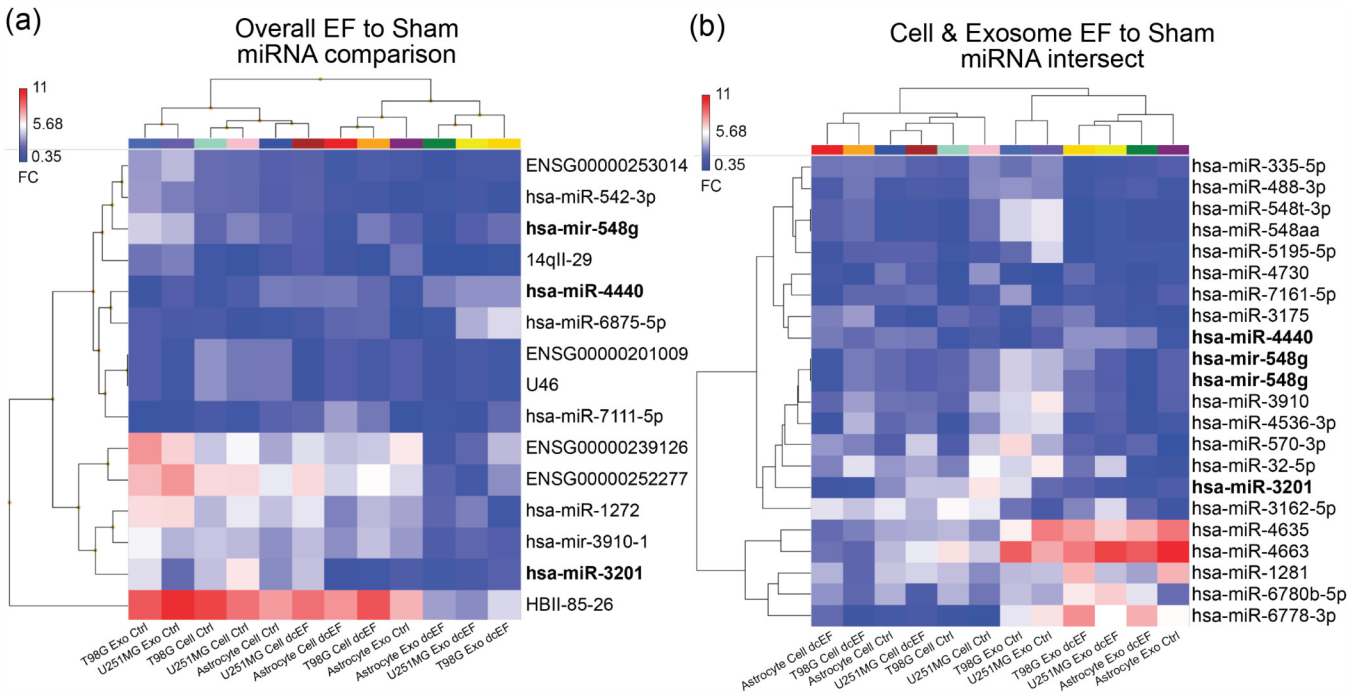

FIG. 6. The hierarchical clustering of (a) small RNA changes compared with overall cellular RNA and exosomal RNA differences between 100 V m^{-1} dcEF stimulation and sham samples and (b) small RNA changes shared among a double intersection and a triple intersection in a Venn diagram between dcEF and sham pairs in cellular and exosomal RNAs when they are analyzed separately. The three miRNAs (hsa-miRNA-4440, hsa-miR-3201, and hsa-mir548g) identified in both analyses were emphasized in bold texts.

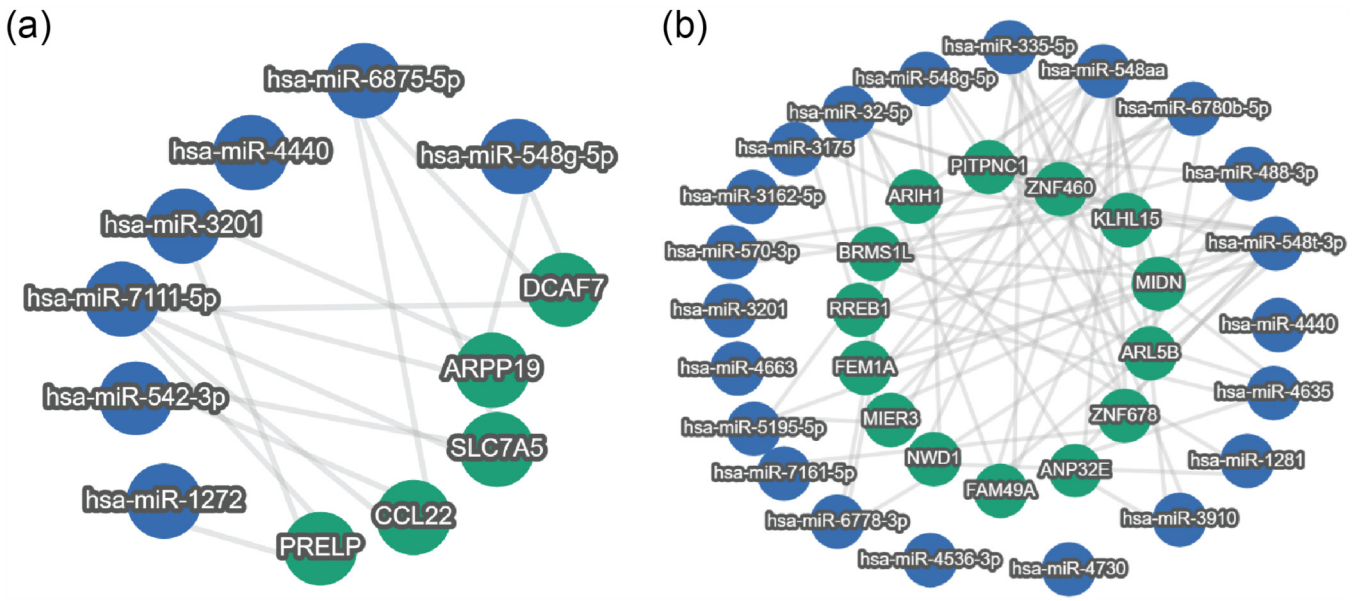

FIG. 7. The signaling targets of the identified miRNAs that changed during 100 V m^{-1} dcEF stimulation discovered by an miRTargetLink2.0 database in (a) overall comparison and (b) separate comparisons that coexist among double intersections and triple intersections in a Venn diagram. The target genes are labeled as green nodes. For clarity, only molecular targets shared by a minimum of three miRNAs in an overall comparison and molecular targets shared by a minimum of five miRNAs in a separate comparison are graphed.

D. Uncovering signaling pathway through dcEF-regulated miRNA expression

The 16 small RNAs identified to have statistically significant changes were further analyzed for target genes and pathways using the miRTargetLink 2.0 Database[52] [see Fig. 7(a)]. To enhance clarity and identify highly connected targets, molecular targets shared by at least three miRNAs were graphed. Notably, dcEF stimulation-regulated miRNAs target five genes: *PRELP*, *CCL22*, *SLC7A5*, *ARPP19*, and *DCAF7*. The molecular target pathways connected to these five genes highlighted by miRTargetLink 2.0 are shown in Fig. S5 of the supplementary material.

IV. DISCUSSIONS

Uniform dcEF stimulation is essential to ensure homogeneous cell pacing and to avoid confounding effects from dielectrophoresis.[33,39] While significant efforts have been made to integrate electrical stimulation into biologist-friendly devices, such as Petri dishes and multi-well plates, many of these systems contain areas where products from unstimulated cells can mix with those from stimulated cells.[37,54–57] In our proposed device, nearly all cells on the culture surface receive highly uniform dcEF stimulation. Moreover, our submersion process ensures a bubble-free device assembly, contributing to cell survival (Fig. 3).

Given the RNA instability and the low abundance of microRNAs, minimizing sample processing time is critical.[58,59] Conventional microfluidic platforms offer uniform electrical pacing to cells, but limited sample accessibility poses challenges for processing-sensitive multi-omics studies. Our reversible-sealing design enables rapid recovery and processing of cells and their products within minutes after the experiment, significantly reducing sample loss. In this study, exosomes were isolated via differential centrifugation of the conditioned medium. Future adaptation of microfluidic devices for online exosome concentration and purification could facilitate rapid analysis of exosomes and exosomal miRNAs, especially when integrated with bioreactors featuring large culture areas.[34]

By differential expression analysis of overall comparison between dcEF stimulation and its control [Fig. 6(a) and Table I], we have identified 16 small RNAs, including 5 snoRNAs, 4 C/D Box RNAs, 2 stem-loop RNAs, and 6 miRNAs. Among these, hsa-miR-4440, hsa-miR-6875-5p, and hsa-miR-7111-5p were up-regulated following dcEF stimulation. hsa-miR-4440 miRNA is known to be expressed differentially in glioblastoma tumors and radioresistant glioblastoma cell populations.[60–62] Interestingly, Alfardus *et al.* reported that hsa-miR-4440 expression was down-regulated by more than 2.6-fold in the invasive regions compared to the core and rim regions of a GBM tissue. If electrical stimulation can influence the infiltrative behavior of GBM, its role in mediating dcEF-GBM interactions warrants further investigation. However, our study did not detect the previously reported tumor-suppressive miRNA-138 in tumor-treating fields, suggesting potential differences in miRNA expression profiles between dcEF and acEF treatments.[63] The expression of hsa-miR-6875-5p and hsa-miR-7111-5p has also been reported to be associated with breast cancer and esophageal squamous cell carcinoma.[64,65]

The molecular mechanisms underlying the up-regulation of these microRNAs by dcEF require further elucidation.

Among the down-regulated small RNAs, two C/D box small nucleolar RNAs, HBII-85-26 and ENSG00000252277, also known as *SNORD*116 − 26 and *SNORD*116 − 30, are highly expressed in glioblastoma cell lines and down-regulated after dcEF stimulation [Fig. 6(a)]. The *SNORD*116 gene is reported to play a vital role in the regulation of human metabolism and a molecular target of the Prader–Willi syndrome.[66,67] Since dcEF stimulation is known to regulate cellular metabolism,[13] exploring the roles of these C/D box genes in dcEF-regulated metabolism presents an intriguing avenue for future research. hsa-miR-3201 miRNA and hsa-mir-548g stem-loop RNA were among the down-regulated RNAs following dcEF stimulation. hsa-miR-3201 miRNA has not been validated in glioblastoma pathogenesis but has been proposed as a bloodborne prognostic marker for hepatocellular carcinoma.[68] hsa-mir-548g, although less studied, has been found to modulate the replication of dengue virus in cells.[69] Other miRNAs from the mir-548 family, such as mir-548aj, mir-548t, mir-548az, and mir-548x, have been associated with proliferation and mobility in glioblastoma cells.[70,71] hsa-miR548t-3p, hsa-miR548aa, and hsa-mir-548g were found to have different expressions among T98G and U251MG cellular miRNA expressions, but the expression of the miRNAs in the exosome decrease in both cell types for more than 1.5-fold (Table I). there is currently no evidence directly linking miRNAs to electrotaxis, the distinct differential expression of miRNAs between EF-treated and Sham samples suggests a need for further exploration into their potential role in the electrotaxis of GBM and its infiltration capabilities.

Five target genes were identified through pathway discovery based on a minimum of three shared targets among the differentially expressed small RNAs in EF vs sham samples [Fig. 7(a)]. None of these genes—*PRELP*, *CCL22*, *ARPP19*, *DCAF7*, and *SLC7A5*—have been previously associated with GBM pathogenesis. *PRELP* exhibits tumor-suppressive properties and mediates interactions between focal adhesions and the extracellular matrix (ECM).[72–74] *CCL22*, a chemokine ligand, regulates signaling pathways within the tumor microenvironment.[75,76] *ARPP19* is implicated in acute myeloid leukemia relapse and plays a role in cell cycle regulation through the cAMP/protein kinase A (PKA) signaling pathway.[77–79] Notably, the cAMP/PKA pathway has been linked to cell fragment electrotaxis.[80,81]

Moreover, two of the targeted genes *DCAF7* and *SLC7A5* have been known to regulate the protein metabolism through the mammalian target of a rapamycin (mTOR) pathway[82,83] and have been implicated in cancer progression.[82,84,85] The mTOR pathway has also been identified as a signaling pathway in glioblastoma electrotaxis.[86] *SLC7A5* additionally regulates the type A voltage-gated potassium channel (VGKC) Kv1.2 and plays a role in neurodevelopmental delay.[87] Kv1.2 is known for maintaining resting membrane potential in the central nervous system and is implicated in electrotaxis.[88] Our previous work on voltage-gated calcium channels (VGCCs) and VGKCs in glioblastoma electrotaxis has shown connections between ion channel expression and clinical outcomes.[50,89] Inhibition of type A VGKCs can mediate glioblastoma cell electrotaxis on the laminin ECM. The findings from this microarray study suggest that voltage-gated ion channels may mediate glioblastoma cell responses to dcEF, warranting further investigation. Calcium signaling in the cardiomyocytes has been reported to affect the alternative splicing activities of RNA polymerase II through histone modification.[90] It would be plausible that electric stimulation-induced ion channel activation could also mediate miRNA biogenesis underlying the differential miRNA expressions under dcEF stimulation.

The signaling pathways contributed by these genes is shown in Fig. S5 of the supplementary material. The differentially expressed miRNAs in the dcEF stimulation are involved in the mediation of signaling pathways associated with metabolic processes and apoptosis.

When cell samples and exosomal samples are separately analyzed for the dcEF stimulation effects, the 21 identified miRNAs are different from those in an overall comparison. This may be due to the inherent difference between cellular RNA and exosomal RNA, where the exosomal miRNA cargo is specialized [Fig. 6(b)] similarly reported elsewhere.[91,92] Glioblastoma tissue-derived exosomes play a crucial role in the progression, resistance emergence, and remodeling of the tumor microenvironment by inducing angiogenesis and immune-modulation.[93,94] The selective packing of different cellular products into exosomes, including miRNAs, can aid in the crosstalk between glioblastoma and nearby tissues or even systemic interactions, such as immunosuppression, through paracrine and autocrine signaling.[95] Further clarification of the genes and the miRNAs targeting them in the pathogenesis of glioblastoma may help identify new therapeutic targets and biomarkers for prognosis.

The 14 target genes identified through pathway discovery based on five shared targets among the differentially expressed small RNAs are shown in Fig. 7(b). Some noteworthy target genes associated with cancer pathogenesis are discussed. *PITPNC1* promotes malignant secretion and drive metastasis in breast cancer, colon cancer, and melanoma.[96] *ARL5B* and *MIER3* are also promoters of an epithelial–mesenchymal transition in breast cancer, and *ZFN460* plays a similar role in gastric cancer.[97–99] *FAM49* is highly expressed in the brain and is associated with the chemotaxis of glioblastoma through activation of Rac1.[100] *BRMS1L* has been reported to have prognostic values for an invasive glioblastoma phenotype.[101] *RREB1*, *ANP32E*, and *ZNF678* have been reported to play a role in maintenance or promotion of a malignant phenotype of a glioblastoma stem cell.[102–104]

V. CONCLUSION

In this study, we designed a reversibly sealed microfluidic dcEF stimulation bioreactor for effective cell stimulation and sample recovery. Our platform provides uniform dcEF stimulation with bubble-free condition, essential for reliable biological studies, and allows for rapid sample processing, minimizing RNA degradation. To discover molecular targets and signaling pathways underlying cell–cell paracrine interactions in bioelectricity, we further utilized the platform to study the microRNA expression in glioblastoma cells, primary astrocytes, and their exosomes with and without dcEF stimulation. To our knowledge, it is the first study comparing differential miRNA expression between dcEF-stimulated cells and exosomes from conditioned media. We identified

significant changes in miRNA expression due to dcEF stimulation, including the up-regulation of hsa-miR-4440 and the down-regulation of hsa-miR-3201 and hsa-mir-548 g. These findings suggest potential molecular targets and pathways involved in glioblastoma's response to dcEF, warranting further investigation.

The versatility of our platform makes it suitable for future dcEF stimulation experiments in multi-omics analyses and tissue engineering, where uniform dcEF pacing and prompt sample recovery are required over large culture areas. In the future, the miRNAs, their molecular targets, and relevant signaling pathways will be explored functionally to investigate their roles in cellular signaling and response to direct current physiological electric field.

SUPPLEMENTARY MATERIAL

See the supplementary material for five supplementary figures and one supplementary table.

ACKNOWLEDGMENTS

The authors thank the Okinawa Institute of Science and Technology Graduate University (OIST) for its financial support with subsidy funding from the Cabinet Office, Government of Japan and the grant support to H.-.F.T. from the National Science and Technology Council, Taiwan and Chang Gung Memorial Hospital (Nos. NSTC112-2221-E-182-012-MY3 and CMRPD1N0351). We are grateful for the support provided by the Sequencing Section and the Imaging Section of Core Facilities at OIST. We thank Dr. Toshio Sasaki for technical support on TEM imaging. The authors also acknowledge the Microscopy Center at Chang Gung University for technical assistance.

AUTHOR DECLARATIONS

Conflict of Interest

The authors have no conflicts to disclose.

Author Contributions

Hsieh-Fu Tsai: Conceptualization (equal); Data curation (equal); Formal analysis (equal); Funding acquisition (equal); Investigation (equal); Methodology (equal); Writing – original draft (equal); Writing – review & editing (equal). **Amy Q. Shen:** Conceptualization (equal); Funding acquisition (equal); Investigation (equal); Project administration (equal); Supervision (equal); Writing – review & editing (equal).

DATA AVAILABILITY

The microarray CEL files of cell and exosome samples have been deposited in the Gene Expression Omnibus (GEO) on the NCBI database (Accession No. GSE2721714).

REFERENCES

[1]M. Levin, Mol. Biol. Cell **25**, 3835 (2014).
[2]T. B. Saw, X. Gao, M. Li, J. He, A. P. Le, S. Marsh, K.-h. Lin, A. Ludwig, J. Prost, and C. T. Lim, Nat. Phys. **18**, 1122 (2022).
[3]G. Shim, I. B. Breinyn, A. Martínez-Calvo, S. Rao, and D. J. Cohen, Nat. Commun. **15**, 2938 (2024).
[4]M. Levin, Cell **184**, 1971 (2021).
[5]L. F. George and E. A. Bates, Front. Cell Dev. Biol. **10**, 772230 (2022).
[6]R. Nuccitelli, *Current Topics in Developmental Biology* (Academic Press, 2003), Vol. 58, pp. 1–26.
[7]M. A. Messerli and D. M. Graham, Biol. Bull. **221**, 79 (2011).
[8]G. Tai, M. Tai, and M. Zhao, Burns Trauma **6**, 20 (2018).
[9]R. Luo, Y. Liang, J. Yang, H. Feng, Y. Chen, X. Jiang, Z. Zhang, J. Liu, Y. Bai, J. Xue, S. Chao, Y. Xi, X. Liu, E. Wang, D. Luo, Z. Li, and J. Zhang, Adv. Mater. **35**, 2208395 (2023).
[10]J. I. Hoare, A. M. Rajnicek, C. D. McCaig, R. N. Barker, and H. M. Wilson, J. Leukoc. Biol. **99**, 1141 (2016).
[11]E. Zimolag, J. Borowczyk-Michalowska, S. Kedracka-Krok, B. Skupien-Rabian, E. Karnas, S. Lasota, J. Sroka, J. Drukala, and Z. Madeja, Biochim. Biophys. Acta, Mol. Cell Res. **1864**, 267 (2017).
[12]M. B. A. Djamgoz, M. Mycielska, Z. Madeja, S. P. Fraser, and W. Korohoda, J. Cell Sci. **114**, 2697 (2001).
[13]M. E. Mycielska and M. B. A. Djamgoz, J. Cell Sci. **117**, 1631 (2004).
[14]S. L. Payne, M. Levin, and M. J. Oudin, Bioelectricity **1**, 114 (2019).
[15]D. Bonazzi and N. Minc, Adv. Wound Care **3**, 139 (2014).
[16]O. Herreras, Front. Neural Circuits **10**, 00101 (2016).
[17]E. Iredale, A. Elsaleh, H. Xu, P. Christiaans, A. Deweyert, J. Ronald, S. Schmid, M. O. Hebb, T. M. Peters, and E. Wong, Phys. Med. Biol. **68**, 308 (2023).
[18]W. Kim, H. Yoo, S. H. Shin, H. S. Gwak, and S. H. Lee, Brain Tumor Res. Treat. **2**, 124 (2014).
[19]M. Kurdi, S. Baeesa, F. Okal, A. K. Bamaga, E. Faizo, A. A. Fathaddin, A. Alkhotani, M. M. Karami, and B. Bahakeem, Cancer Rep. **6**, e1905 (2023).
[20]O. Rominiyi, A. Vanderlinden, S. J. Clenton, C. Bridgewater, Y. Al-Tamimi, and S. J. Collis, Br. J. Cancer **124**, 697 (2021).
[21]J. M. Pitt, G. Kroemer, and L. Zitvogel, J. Clin. Investig. **126**, 1139 (2016).
[22]G. Berumen Sánchez, K. E. Bunn, H. H. Pua, and M. Rafat, Cell Commun. Signal. **19**, 104 (2021).
[23]S. Gurung, D. Perocheau, L. Touramanidou, and J. Baruteau, Cell Commun. Signal. **19**, 47 (2021).
[24]D. Barh, B. Kamapantula, N. Jain, J. Nalluri, A. Bhattacharya, L. Juneja, N. Barve, S. Tiwari, A. Miyoshi, V. Azevedo, K. Blum, A. Kumar, A. Silva, and P. Ghosh, Sci. Rep. **5**, 12832 (2015).
[25]A. Matsuda, I. K. Yan, C. Foye, M. Parasramka, and T. Patel, Best Pract. Res. Clin. Endocrinol. Metab. **30**, 577 (2016).
[26]A. Buruiană, I. Florian, A. I. Florian, T.-L. Timiș, C. M. Mihu, M. Micläuș, S. Oșan, I. Hrapșa, R. C. Cataniciu, M. Farcaș, and Ș. Susman, Int. J. Mol. Sci. **21**, 1950 (2020).
[27]I. Conti, G. Varano, C. Simioni, I. Laface, D. Milani, E. Rimondi, and L. M. Neri, Cells **9**, 220 (2020).
[28]J. Makarova, A. Turchinovich, M. Shkurnikov, and A. Tonevitsky, Trends Biochem. Sci. **46**, 640 (2021).
[29]P. M. McDonough and C. C. Glembotski, J. Biol. Chem. **267**, 11665 (1992).
[30]M. Marotta, R. Bragós, and A. M. Gómez-Foix, BioTechniques **36**, 68 (2004).
[31]J. T. Maxwell, D. Trac, M. Shen, M. E. Brown, M. E. Davis, M. S. Chao, K. J. Supapannachart, C. A. Zaladonis, E. Baker, M. L. Li, J. Zhao, and D. I. Jacobs, Stem Cells **37**, 1528 (2019).
[32]H. Takaya, M. Comtois-Bona, A. Spasojevic, D. Cortes, F. Variola, W. Liang, M. Ruel, E. J. Suuronen, and E. I. Alarcon, Front. Bioeng. Biotechnol. **11**, 1253602 (2023).
[33]H.-F. Tsai, J.-Y. Cheng, H.-F. Chang, T. Yamamoto, and A. Q. Shen, Sci. Rep. **6**, 26222 (2016).
[34]S. M. Mousavi, S. M. A. Mahdian, M. S. Ebrahimi, M. Taghizadieh, M. Vosough, J. S. Nahand, S. Hosseindoost, N. Vousooghi, H. A. Javar, B. Larijani, M. R. Hadjighassem, N. Rahimian, M. R. Hamblin, and H. Mirzaei, Mol. Ther. Nucleic Acids **28**, 758 (2022).
[35]M. Zhao, Semin. Cell Dev. Biol. **20**, 674 (2009).
[36]Y.-S. Sun, Sensors **17**, 2048 (2017).

[37]C. N. M. Ryan, M. N. Doulgkeroglou, and D. I. Zeugolis, BMC Biomed. Eng. **3**, 1 (2021).
[38]C.-W. Huang, H.-Y. Chen, M.-H. Yen, J. J. W. Chen, T.-H. Young, and J.-Y. Cheng, PLoS One **6**, e25928 (2011).
[39]H.-F. Tsai, C.-W. Huang, H.-F. Chang, J. J. W. Chen, C.-H. Lee, and J.-Y. Cheng, PLoS One **8**, e73418 (2013).
[40]R. Ma, J. Liang, W. Huang, L. Guo, W. Cai, L. Wang, C. Paul, H.-T. Yang, H. W. Kim, and Y. Wang, Antioxid. Redox Signal. **28**, 371 (2018).
[41]Y. Ma, C. Yang, Q. Liang, Z. He, W. Weng, J. Lei, L. Skudder-Hill, J. Jiang, and J. Feng, Mol. Neurobiol. **59**, 3665 (2022).
[42]L.-L. Pan, J.-Q. Ke, C.-C. Zhao, S.-Y. Huang, J. Shen, X.-X. Jiang, and X.-T. Wang, PLoS One **11**, e0152525 (2016).
[43]X. Quan, L. Huang, Y. Yang, T. Ma, Z. Liu, J. Ge, J. Huang, and Z. Luo, Neurochem. Res. **42**, 513 (2017).
[44]N. Selvamurugan, Z. He, D. Rifkin, B. Dabovic, and N. C. Partridge, Stem Cells Int. **2017**, 2450327.
[45]J. Shen, X. Nie, S.-Y. Huang, Y.-Q. Qin, L.-L. Pan, and X.-T. Wang, Biochem. Biophys. Res. Commun. **509**, 1021 (2019).
[46]C. G. Vann, X. Zhang, A. Khodabukus, M. C. Orenduff, Y.-H. Chen, D. L. Corcoran, G. A. Truskey, N. Bursac, and V. B. Kraus, Front. Physiol. **13**, 937899 (2022).
[47]N. Kawanishi, T. Tominaga, and K. Suzuki, Am. J. Physiol. Regul. Integr. Comp. Physiol. **324**, R761 (2023).
[48]E. H. Kim, Y. Jo, S. Sai, M.-J. Park, J.-Y. Kim, J. S. Kim, Y.-J. Lee, J.-M. Cho, S.-Y. Kwak, J.-H. Baek, Y. K. Jeong, J.-Y. Song, M. Yoon, and S.-G. Hwang, Oncogene **38**, 6630 (2019).
[49]Y. Liu, W.-b. Liu, K.-j. Liu, L. Ao, J. Cao, J. L. Zhong, and J.-y. Liu, PLoS One **10**, e0139949 (2015).
[50]H.-F. Tsai, C. IJspeert, and A. Q. Shen, APL Bioeng. **4**, 036102 (2020).
[51]M. E. Ritchie, B. Phipson, D. Wu, Y. Hu, C. W. Law, W. Shi, and G. K. Smyth, Nucleic Acids Res. **43**, e47 (2015).
[52]F. Kern, E. Aparicio-Puerta, Y. Li, T. Fehlmann, T. Kehl, V. Wagner, K. Ray, N. Ludwig, H.-P. Lenhof, E. Meese, and A. Keller, Nucleic Acids Res. **49**, W409 (2021).
[53]T. Nedachi, H. Fujita, and M. Kanzaki, Am. J. Physiol. Endocrinol. Metab. **295**, E1191 (2008).
[54]G. M. Xiong, A. T. Do, J. K. Wang, C. L. Yeoh, K. S. Yeo, and C. Choong, J. Biol. Eng. **9**, 14 (2015).
[55]S. Mobini, L. Leppik, and J. H. Barker, BioTechniques **60**, 95 (2016).
[56]J. C. Silva, J. Meneses, F. F. F. Garrudo, S. R. Fernandes, N. Alves, F. C. Ferreira, and P. Pascoal-Faria, Sci. Rep. **14**, 5458 (2024).
[57]M. Solazzo and M. G. Monaghan, ACS Biomater. Sci. Eng. **9**, 4573 (2023).
[58]P. Chugh and D. P. Dittmer, Wiley Interdiscip. Rev. RNA **3**, 601 (2012).
[59]L. Moldovan, K. E. Batte, J. Trgovcich, J. Wisler, C. B. Marsh, and M. Piper, J. Cell Mol. Med. **18**, 371 (2014).
[60]J. Ondracek, P. Fadrus, J. Sana, A. Besse, T. Loja, M. Vecera, L. Radova, M. Smrcka, P. Slampa, and O. Slaby, Anticancer Res. **37**, 1099 (2017).
[61]H. Alfardus, M. de Los Angeles Estevez-Cebrero, J. Rowlinson, A. Aboalmaaly, A. Lourdusamy, S. Abdelrazig, C. Ortori, R. Grundy, D.-H. Kim, A. McIntyre, and S. Smith, Sci. Rep. **11**, 15908 (2021).
[62]V. Bafiti, S. Ouzounis, E. Siapi, I. M. Grypari, A. Theofanopoulos, V. Panagiotopoulos, V. Zolota, D. Kardamakis, and T. Katsila, Metabolites **13**, 362 (2023).
[63]M. Yeh, Y.-Y. Wang, J. Y. Yoo, C. Oh, Y. Otani, J. M. Kang, E. S. Park, E. Kim, S. Chung, Y.-J. Jeon, G. A. Calin, B. Kaur, Z. Zhao, and T. J. Lee, Sci. Rep. **11**, 9219 (2021).
[64]X. Cui, Z. Li, Y. Zhao, A. Song, Y. Shi, X. Hai, and W. Zhu, PeerJ **6**, e4551 (2018).
[65]Z. Ma, T. Zhu, H. Wang, B. Wang, L. Fu, and G. Yu, J. Biochem. **172**, 29 (2022).
[66]Y. Qi, L. Purtell, M. Fu, N. J. Lee, J. Aepler, L. Zhang, K. Loh, R. F. Enriquez, P. A. Baldock, S. Zolotukhin, L. V. Campbell, and H. Herzog, Sci. Rep. **6**, 18614 (2016).
[67]L. Baldini, A. Robert, B. Charpentier, and S. Labialle, Mol. Biol. Evol. **39**, msab348 (2021).
[68]L. Grisetti, N. V. T. Võ, N. N. Q. Nguyn, L. S. Crocé, A. Visintin, C. Tiribelli, and D. Pascut, Technol. Cancer Res. Treat. **21**, 15330338221132924 (2022).
[69]W. Wen, Z. He, Q. Jing, Y. Hu, C. Lin, R. Zhou, X. Wang, Y. Su, J. Yuan, Z. Chen, J. Yuan, J. Wu, J. Li, X. Zhu, and M. Li, J. Infect. **70**, 631 (2015).
[70]M. A. Calhoun, Y. Cui, E. E. Elliott, X. Mo, J. J. Otero, and J. O. Winter, Sci. Rep. **10**, 311 (2020).
[71]M. R. Kalhori, E. Arefian, F. Fallah Atanaki, K. Kavousi, and M. Soleimani, Sci. Rep. **10**, 1558 (2020).
[72]E. Bengtsson, K. Lindblom, V. Tillgren, and A. Aspberg, Biochem. J. **473**, 1153 (2016).
[73]J. Hopkins, K. Asada, A. Leung, V. Papadaki, H. Davaapil, M. Morrison, T. Orita, R. Sekido, H. Kosuge, M. A. Reddy, K. Kimura, A. Mitani, K. Tsumoto, R. Hamamoto, M. S. Sagoo, and S.-i. Ohnuma, Cancers **14**, 4926 (2022).
[74]A. Dozen, K. Shozu, N. Shinkai, N. Ikawa, R. Aoyama, H. Machino, K. Asada, H. Yoshida, T. Kato, R. Hamamoto, S. Kaneko, and M. Komatsu, J. Pers. Med. **12**, 1999 (2022).
[75]Y.-H. Chen, B.-Y. Zhou, X.-J. Wu, J.-F. Xu, J.-A. Zhang, Y.-H. Chen, and S.-S. Liang, Oncol. Rep. **36**, 2017 (2016).
[76]I. Lecoq, K. L. Kopp, M. Chapellier, P. Mantas, E. Martinenaite, M. Perez-Penco, L. Rønn Olsen, M.-B. Zocca, A. Wakatsuki Pedersen, and M. H. Andersen, OncoImmunology **11**, 2115655 (2022).
[77]A. Dupré, E. M. Daldello, A. C. Nairn, C. Jessus, and O. Haccard, Nat. Commun. **5**, 3318 (2014).
[78]K. Hached, P. Goguet, S. Charrasse, S. Vigneron, M. P. Sacristan, T. Lorca, and A. Castro, J. Cell Biol. **218**, 541 (2019).
[79]E. Mäkelä, E. Löyttyniemi, U. Salmenniemi, O. Kauko, T. Varila, V. Kairisto, M. Itälä-Remes, and J. Westermarck, Cancers **11**, 1774 (2019).
[80]C. E. Pullar and R. R. Isseroff, J. Cell Sci. **118**, 2023 (2005).
[81]K. Zhu, Y. Sun, A. Miu, M. Yen, B. Liu, Q. Zeng, A. Mogilner, and M. Zhao, J. Cell Physiol. **231**, 1291 (2016).
[82]J. Xu, Z. Ye, Q. Zhuo, H. Gao, Y. Qin, X. Lou, W. Zhang, F. Wang, Y. Wang, D. Jing, G. Fan, Y. Zhang, X. Chen, J. Chen, X. Xu, X. Yu, and S. Ji, Cancer Res. **83**, 2226 (2023).
[83]A. M. Sokolov, J. C. Holmberg, and D. M. Feliciano, Hum. Mol. Genet. **29**, 3003 (2020).
[84]T. Hisada, N. Kondo, Y. Wanifuchi-Endo, S. Osaga, T. Fujita, T. Asano, Y. Uemoto, S. Nishikawa, Y. Katagiri, M. Terada, A. Kato, H. Sugiura, K. Okuda, H. Kato, M. Komura, S. Morita, S. Takahashi, and T. Toyama, Sci. Rep. **12**, 16515 (2022).
[85]D. Jia, L. Li, P. Wang, Q. Feng, X. Pan, P. Lin, S. Song, L. Yang, and J. Yang, Front. Oncol. **12**, 1043177 (2022).
[86]J. G. Lyon, S. L. Carroll, N. Mokarram, and R. V. Bellamkonda, Sci. Rep. **9**, 5309 (2019).
[87]V. A. Baronas, R. Y. Yang, L. C. Morales, S. Sipione, and H. T. Kurata, Nat. Commun. **9**, 4417 (2018).
[88]G. Zhang, M. Edmundson, V. Telezhkin, Y. Gu, X. Wei, P. J. Kemp, and B. Song, J. Cell Physiol. **231**, 1375 (2016).
[89]R. Wang, C. I. Gurguis, W. Gu, E. A. Ko, I. Lim, H. Bang, T. Zhou, and J.-H. Ko, Sci. Rep. **5**, 11593 (2015).
[90]A. Sharma, H. Nguyen, C. Geng, M. N. Hinman, G. Luo, and H. Lou, Proc. Natl. Acad. Sci. U.S.A. **111**, E4920 (2014).
[91]A. Abramowicz, W. Łabaj, J. Mika, K. Szołtysek, I. Ślezak Prochazka, Ł Mielańzyk, M. D. Story, M. Pietrowska, A. Polański, and P. Widłak, Radiat. Res. **194**, 133 (2020).
[92]K. Asgarpour, Z. Shojaei, F. Amiri, J. Ai, M. Mahjoubin-Tehran, F. Ghasemi, R. ArefNezhad, M. R. Hamblin, and H. Mirzaei, Cell Commun. Signal. **18**, 149 (2020).
[93]R. Isaac, F. C. G. Reis, W. Ying, and J. M. Olefsky, Cell Metab. **33**, 1744 (2021).

[94]S. N. Mousavikia, L. Darvish, M. T. Bahreyni Toossi, and H. Azimian, Life Sci. **350**, 122743 (2024).
[95]B. T. Himes, P. A. Geiger, K. Ayasoufi, A. G. Bhargav, D. A. Brown, and I. F. Parney, Front. Oncol. **11**, 770561 (2021).
[96]N. Halberg, C. A. Sengelaub, K. Navrazhina, H. Molina, K. Uryu, and S. F. Tavazoie, Cancer Cell **29**, 339 (2016).
[97]Y. Xu, S. Ye, N. Zhang, S. Zheng, H. Liu, K. Zhou, L. Wang, Y. Cao, P. Sun, and T. Wang, Cancer Commun. **40**, 484 (2020).
[98]W. Huang, J. Chen, X. Liu, X. Liu, S. Duan, L. Chen, X. Liu, J. Lan, Y. Zou, D. Guo, and J. Zhou, Exp. Cell Res. **406**, 112722 (2021).
[99]L. An and Y. Liu, Exp. Cell Res. **422**, 113452 (2023).
[100]L. Fort, J. M. Batista, P. A. Thomason, H. J. Spence, J. A. Whitelaw, L. Tweedy, J. Greaves, K. J. Martin, K. I. Anderson, P. Brown, S. Lilla, M. P. Neilson, P. Tafelmeyer, S. Zanivan, S. Ismail, D. M. Bryant, N. C. O. Tomkinson, L. H. Chamberlain, G. S. Mastick, R. H. Insall, and L. M. Machesky, Nat. Cell Biol. **20**, 1159 (2018).
[101]J. Feldheim, A. F. Kessler, J. J. Feldheim, D. Schmitt, C. Oster, L. Lazaridis, M. Glas, R.-I. Ernestus, C. M. Monoranu, M. Löhr, and C. Hagemann, Cancers **15**, 2907 (2023).
[102]A. D. Berezovsky, L. M. Poisson, D. Cherba, C. P. Webb, A. D. Transou, N. W. Lemke, X. Hong, L. A. Hasselbach, S. M. Irtenkauf, T. Mikkelsen, and A. C. deCarvalho, Neoplasia **16**, 193 (2014).
[103]H. Li, Y. Jiang, J. Hu, J. Xu, L. Chen, G. Zhang, J. Zhao, S. Zong, Z. Guo, X. Li, X. Zhao, and Z. Jing, Cell Death Dis. **14**, 23 (2023).
[104]H. Yan, J. Zhu, Y. Ping, M. Yan, G. Liao, H. Yuan, Y. Zhou, F. Xiang, B. Pang, J. Xu, and L. Pang, Stem Cells **41**, 111 (2023).